JOURNAL OF AIRCRAFT
Vol. 46, No. 4, July–August 2009

Experimental Study of a Ground Vortex

Jorge M. M. Barata,* Samuel Ribeiro,† Pedro Santos,† and André R. R. Silva‡
Universidade Beira Interior, 6201-001 Covilhã, Portugal

DOI: 10.2514/1.36619

Laser-Doppler measurements of the mean and turbulent components of the velocity flowfield resulting from the frontal collision of a wall jet with a boundary layer are presented and discussed, together with the visualization of the flow with direct photography and digital film imaging. The experiments were carried out for boundary-layer-to-wall-jet velocity ratios of 0.5 and 0.58. The results revealed the existence of a small counter-rotating recirculating zone located upstream (in the sense of the wall-jet flow) of the separation point, not reported before for this type of flow. This secondary vortex has an oscillating behavior observed in other ground-vortex flows, similar to that which can be observed, namely, through the bimodal histogram of the horizontal velocity (parallel to the wall) measurements, although the power spectra measurements do not exhibit any particular peaks.

Nomenclature

D	=	diameter of the jet at the nozzle exit (short/vertical takeoff and landing application)
f	=	frequency of oscillation of the ground vortex
H	=	height of the rectangular jet nozzle slit (present geometry)
h	=	distance from the nozzle exit to the ground plane
h_v	=	ground-vortex height
U_j	=	velocity of the wall jet
U_0	=	boundary layer or crossflow velocity
u, U, u'	=	instantaneous, mean, and turbulent horizontal velocity components ($u = U + u'$)
$\overline{u'v'}$	=	Reynolds shear stress
u'_{rms}	=	root mean square of the horizontal fluctuating velocity component ($\sqrt{\overline{u'^2}}$, square root of the horizontal Reynolds stress)
V_j	=	velocity of the jet at the nozzle exit (impinging-jet configuration)
V_R	=	boundary-layer-to-wall-jet (or crossflow-to-jet) velocity ratio (U_0/U_j)
v, V, v'	=	instantaneous, mean, and turbulent horizontal velocity components ($v = V + v'$)
v'_{rms}	=	root mean square of the vertical fluctuating velocity component ($\sqrt{\overline{v'^2}}$, square root of the horizontal Reynolds stress)
X	=	horizontal Cartesian coordinate (parallel to the wall, pointing in the sense of the jet)
Y	=	vertical Cartesian coordinate (normal to the wall pointing upward)
δ	=	boundary-layer thickness

I. Introduction

HIGLY curved flows are quite common in nature and are frequently originated by impermeable surfaces that deflect a flow [1]. Flows of this type are characterized by complex phenomena such as extra rates of strain and enhanced turbulence production due to the interaction of normal stresses with normal strains. They can be found in impingement cooling applications in industry, as well as in the flow beneath a short/vertical takeoff and landing (VSTOL) aircraft lifting off or landing with zero or small forward momentum. In the latter application, the impingement of a lift jet on the ground results in the formation of a wall jet that flows radially from the impinging point along the ground surface and interacts strongly with the aircraft, resulting in lift losses, enhanced entrainment close to the ground (suckdown), engine thrust losses following reingestion of the exhaust gases, and possible aerodynamic instabilities caused by fountain impingement on the aircraft underside. The interaction of this wall jet with a freestream flowing parallel to the wall in the opposite sense (crossflow), such as wind, results in the formation of a highly curved flow (ground vortex) far upstream of the impinging jet (from the perspective of the boundary-layer flow) that has profound influences on the flow development [2–7]. Measurements of this type of flow are very scarce in the literature, and those that have been reported are focused on the study of a secondary flow within the impinging-jet flow problem and are dispersed among many different configurations and operating conditions.

Most studies published so far with relevance for the V/STOL problem consider only small impinging distances $h/D < 8$ and low crossflow-to-jet velocity ratios $V_R < 0.1$ (Figs. 1a and 1b). Some information relevant to the flow beneath a V/STOL aircraft in ground vicinity has been provided for some limiting cases, such as $h/D=$ 0.4, but only in the absence of a crossflow (i.e., only for $V_R = 0$) [8,9]. Others studied the interaction of the crossflow with solid surfaces near the nozzle jet exit, such as the underside of the aircraft fuselage and wings (Fig. 1b) [2,4].

Among the studies that do not consider the presence of a surface at the jet exit (Fig. 1a), there is some agreement on the fact that the flow includes large-scale, probably coherent, unsteadiness, although there is no consensus on its causes. Reference [6] reports velocity frequency spectra (obtained with hot-wire measurements) with broadband humps [indicating very-low-frequency unsteadiness ($f = 4$ Hz for $h/D = 3$ and $U_e = 0.1$)] that were attributed to the large-scale "puffing" oscillation (low-frequency pulsating behavior) of the ground vortex and were accompanied by significant variations in the size of the ground vortex. This phenomenon was found to be correlated with disturbances either in the crossflow or in the jet. Therefore, the puffing oscillation was attributed to gross features of the ground-vortex flowfield itself, such as the observed irregularities of its growth and breakup. This unsteadiness was also found to lead to large fluctuations in the height h_v of the vortex, which reaches more that 8 jet diameters for $V_R = 0.05$, increasing with decreasing frequency f, the latter tending almost linearly to zero with V_R. Reference [10] also reports a distinct frequency of oscillation for the

Presented as Paper 343 at the 46th AIAA Aerospace Sciences Meeting and Exhibit, Reno, NV, 7–10 January 2008; received 11 January 2008; revision received 23 November 2008; accepted for publication 25 November 2008.

*Full Professor, Aerospace Sciences Department, Rua Marques Avila e Bolama. Associate Fellow AIAA.
†M.Sc. Student, Aerospace Sciences Department, Rua Marques Avila e Bolama.
‡Assistant Professor, Aerospace Sciences Department, Rua Marques Ávila e Bolama. Member AIAA.

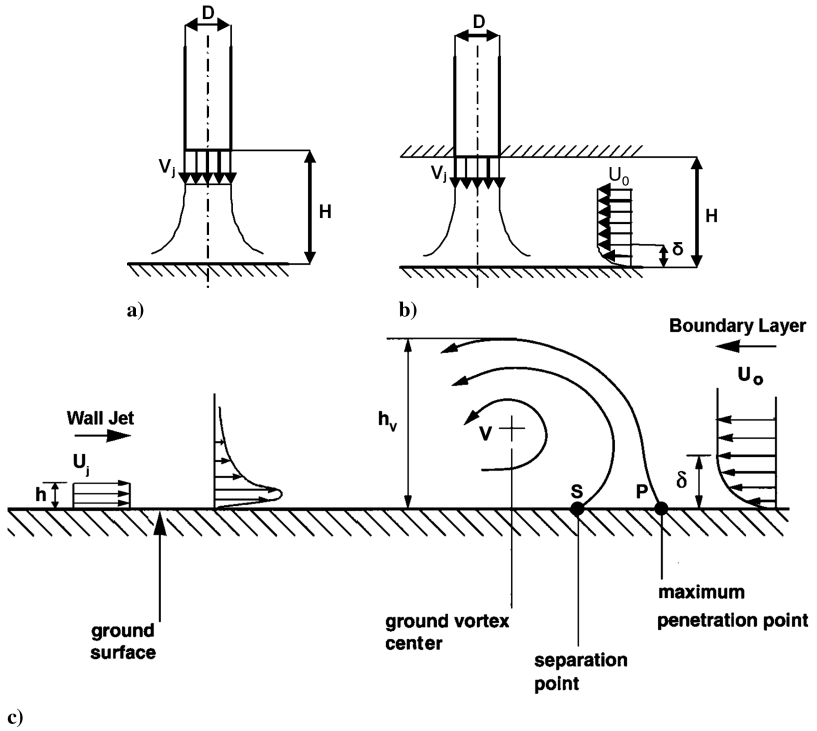

Fig. 1 Diagrams of the various geometries studied: a) jet normal to the wall, b) jet normal to the wall with confinement and crossflow, and c) jet parallel to the wall against a boundary layer (present study).

case of a fountain flow resulting from two compressible impinging jets with nozzle pressure ratios between 1.05 and 4 and impingement height $h/D = 4.4$.

The studies for the lowest values of the velocity ratio V_R, with an upper wall at the jet (or jets), which confines the flow (Fig. 1b), can be found in [2–4,11–14] for single-, twin-, and three-jet configurations. These studies report numerical and experimental results obtained with laser-Doppler velocimetry (LDV) for velocity ratios $V_R =$ 0.014, 0.024, and 0.033 and impingement height $h/D = 3$, 4, and 5. They perform a through analysis of the turbulence structure of the impinging jet and ground-vortex zones, in which no bimodal LDV histograms of velocity are observed, such as could be associated with the kind of instability of puffing oscillations. This is surprising only at first sight, because puffing oscillation of the ground vortex has only been reported for unconfined impinging-jet configurations. In fact, extrapolating the data of [6] for unconfined geometries to the case considered in [3], a ground-vortex puffing frequency $f = 0.2$ Hz is obtained for $V_R = 0.033$, but was not noticeable in LDV measurements using samples of 10,000 points at a acquisition rate of about 100 Hz. The same extrapolation for the ground-vortex height leads to $h/D = 3.5$ to 9.5, which is larger than the distance h/D between the upper and lower plates that confine the crossflow.

Reference [14] further reports that the shape, size, and location of the ground vortex depend on the velocity ratio V_R according with two different regimes. In the first regime (high V_R), the ground vortex and the impinging jet are in contact, whereas in the second regime (lower V_R), the ground vortex is detached and upstream of the impinging zone. It is also observed that the crossflow accelerates above the ground vortex, due to a blockage effect, in a way that is directly connected with the jet exit velocity V_j, and the influence of the upstream wall jet is not limited to the ground vortex but continues upward due to a mechanism not yet understood. The results do not make perceptible any oscillation of the ground vortex, which seems to indicate that the confinement, parameterized by h/D, inhibits the instabilities of the ground vortex.

The present research program is dedicated to the identification of the parameters and regimes associated with instabilities and other secondary effects of a particular ground-vortex flow. To avoid the influence of the impinging region, a plane wall jet is directly produced using a configuration inspired in a previous study of two-dimensional upwash flows (see [15]). The wall jet collides frontally with a boundary layer flowing in the opposite sense produced in a conventional wind tunnel, for variable velocity ratios V_R (Fig. 1c). This research program deepens that of [16], which detected a small recirculation zone located upstream (relative to the wall jet) the separation point for the first time in this type of flow.

II. Experimental Method and Procedures

The wind-tunnel facility designed and constructed for the present study is diagrammed in Fig. 1 and shown in Fig. 2. The recommendations of [17] for open-circuit wind tunnels were followed throughout all the design process, especially for the boundary-layer part of the flow. A fan of 15 kW nominal power drove a maximum flow of 3000 m^3/h through the boundary layer and the wall-jet tunnels of 300×400 mm and 40×400 mm exit sections, respectively. The facility was built to allow variable heights of the wall-jet exit from 15 up to 40 mm.

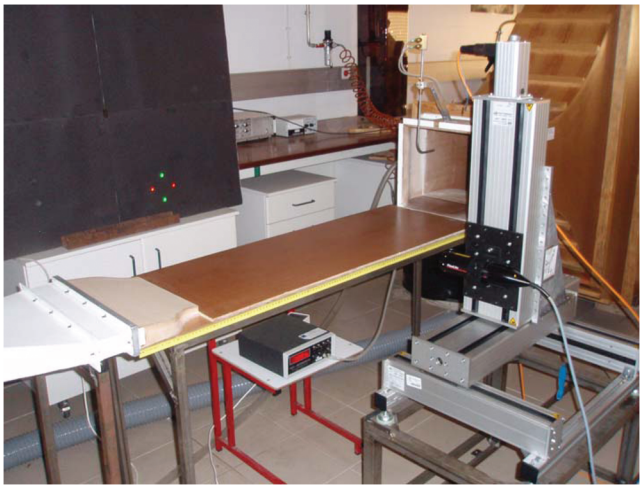

Fig. 2 Photograph of the experimental rig.

Table 1 Principal characteristics of the 2-D laser-Doppler velocimeter

	He-Ne laser	Diode laser
Wave length λ, nm	633	532
Focal length of focusing lens f, mm	400	400
Beam diameter at e^{-2} intensity, mm	1.35	1.35
Beam spacing s, mm	38.87	39.13
Calculated half-angle of beam intersection, θ, deg	2.78	2.8
Fringe spacing δ_f, μm	6.53	5.45
Velocimeter transfer constant K, MHz/ms^{-1}	0.153	0.183

The origin of the horizontal X and vertical Y coordinates was taken near the visual maximum penetration point. The X coordinate is positive in the wall-jet flow direction and Y is positive upward.

The present results were obtained at the vertical plane of symmetry for a wall jet with mean velocities of $U_j = 6$ and 13.7 m/s and mean boundary-layer velocities of $U_o = 3.48$ and 6.9 m/s, corresponding to velocity ratios U_e of 0.58 and 0.50, respectively.

The velocity field was measured with a laser-Doppler velocimeter (Dantec Flowlite 2-D), which comprised a 10 mW He-Ne laser and a 25 mW diode-pumped frequency-doubled Nd:YAG laser, with sensitivity to the flow direction provided by frequency shifting from a Bragg cell at $f_o = 40$ MHz, a transmission, and a backward-scattered light collection focal lens of 400 mm. The half-angle between the beams was 2.8 deg and the calculated dimensions of the axis of the measuring ellipsoid volume at the e^{-2} intensity locations were $135 \times 6.54 \times 6.53$ μm and $112 \times 5.46 \times 5.45$ μm, respectively.

The horizontal U and vertical V mean and turbulent velocities together with the Reynolds shear stress $\overline{u'v'}$ were determined by a two-velocity-channel Dantec BSA F60 processor. The principal characteristics of the laser-Doppler velocimeter are summarized in Table 1. The seeding of the flow with glycerin particles of 0.1–5 μm was produced with medical atomizers operating at 1.5 bar. The transmitting and collecting optics were mounted on a three-dimensional transversing unit, allowing the positioning of the center of the control volume within ± 0.1 mm.

III. Results and Discussion

Experimental visualization studies were first performed using a direct digital photography and a smoke generator to produce the tracer particles. The visualization results of the present complex flow were used to provide a first insight into the nature of the flow and to guide the choice of quantitative measurement locations. The wall jet collides with the boundary layer and is strongly deflected backward with an angle of 36 deg with the ground surface (see Figs. 3 and 4).

Figure 4 shows the measured velocity field and the corresponding streamlines in the vertical plane of symmetry, which shows clearly the upward-deflected flow due to the collision of the wall jet and the boundary layer. The visualization picture is also shown in this figure,

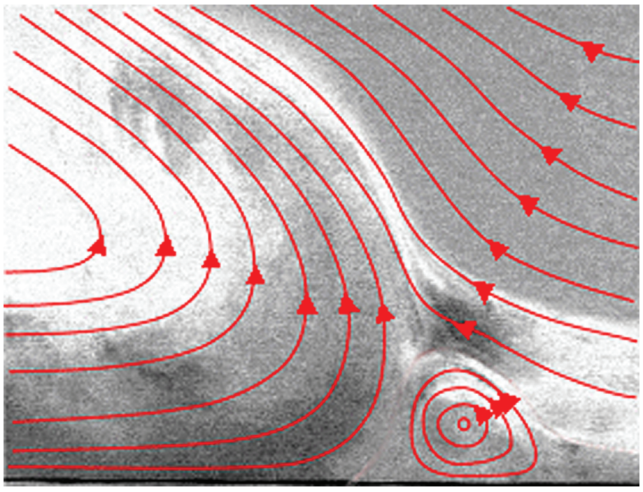

Fig. 5 Visualization of the small vortex and drawing of possible streamlines for $V_R = 0.58$.

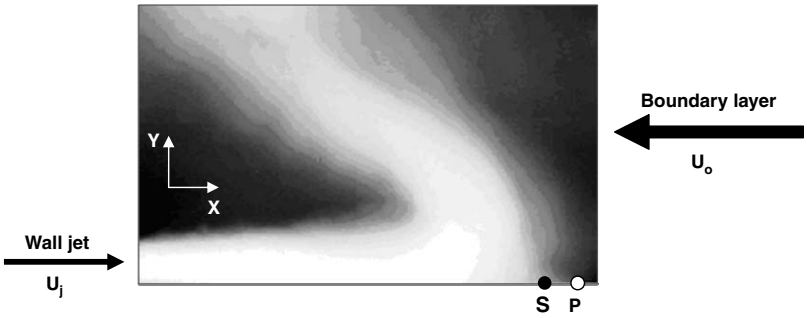

Fig. 3 Visualization of the flow in the impinging zone for $V_R = 0.58$.

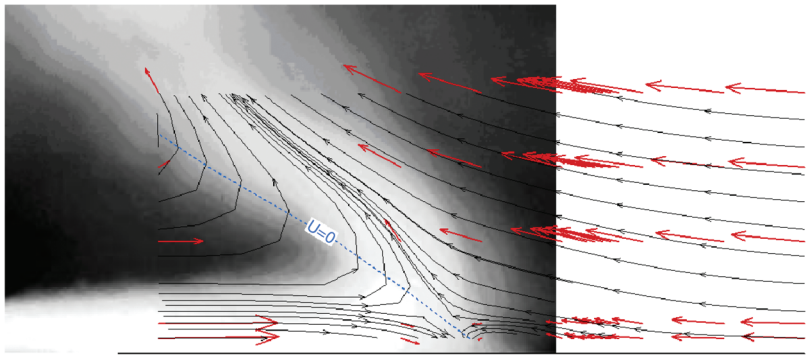

Fig. 4 Visualization of the flow with direct photography, with representation of the measured velocity field and the corresponding calculated stream trace lines for $V_R = 0.58$.

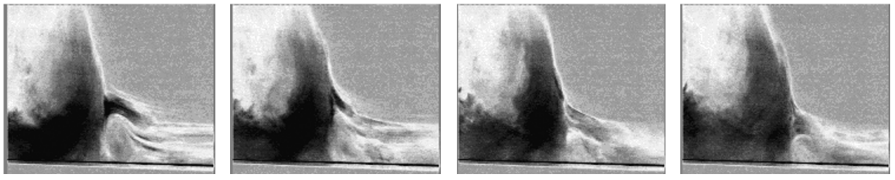

a) b) c) d)

Fig. 6 Small vortex burst and new vortex growth for $V_R = 0.58$ at frames instants $t = 0$, 1/25, 2/25, and 3/25 s.

which confirms the nature of the flow. In the collision zone, both wall jet and boundary-layer fluid moves toward the wall, giving rise to an extremely complex flow, which includes a small secondary-vortex flow near the separation point, probably due to the rollup of the vorticity of the boundary layer.

More detailed visualization studies were performed with a digital camera (Sony DCR-VX2100 PAL). Illumination of the flow was achieved by a sheet of light, about 3 mm thick, obtained by spreading a laser beam with a cylindrical lens. The camera shutter speed was set to 25 frames/s to the best compromise between image contrast and time integration of tracer-particle velocities. The visualization movie was analyzed in detail with Adobe Premiere software, which allowed a frame-by-frame treatment to enhance the flow structures.

Figure 5 was obtained with the method described in the previous paragraph, with some lines drawn to allow a better identification of the small front vortex, which can be observed in the right side of the curved flow. For the present conditions of $V_R = 0.58$, this vortex exists most of the time (about 90% of the frames of the movie), but is highly unstable, with its shape, size, and location varying almost constantly. The behavior of this small vortex is quite similar to the puffing of the ground vortex, as reported by [6], and is illustrated in Fig. 6 with frame instants of 1/25 s. First, the vortex is very small but growing. The lower part of the boundary layer with anticlockwise vorticity seems to merge into the growing vortex. As the small vortex continues to grow, it becomes higher than the boundary layer and breaks up suddenly while is convected upward in the direction of the curved flow. Then a new small vortex appears and starts to grow, and the cyclic process repeats itself (at a frequency of about 8.33 Hz). Reference [6] attributes the vortex growth to the shear-layer vortices, which convect with the wall jet and merge into the ground vortex. In the present case, according to the results of [6], an oscillating frequency of f between 4.2 and 8.6 Hz would be expected, which includes the observed value of 8.33 Hz (from the visualization results). Nevertheless, there is a substantial difference: although the secondary vortex has the same sign of vorticity, it cannot merge into the deflected flow resulting from the collision of the wall jet with the boundary layer, because the vertical velocity component is always positive above the vortex. So the unsteadiness reported before is probably due to an additional small vortex upstream of the ground vortex that, due to its extremely small size, could not be observed so far, as in the case of small crossflow-to-jet velocity ratios [2–4,11–14].

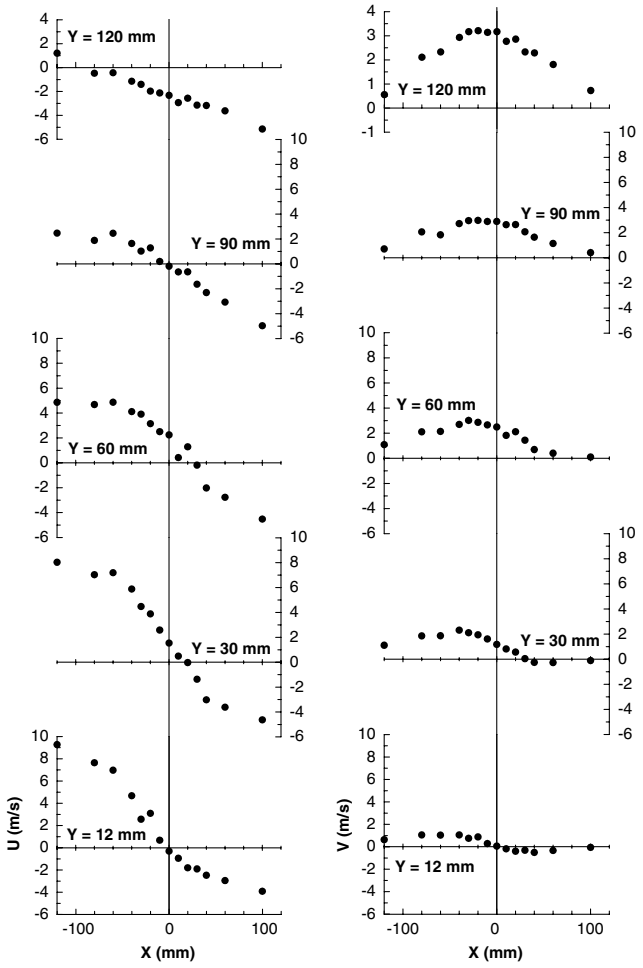

a) b)

Fig. 7 Horizontal profiles of the mean velocity characteristics for $V_R = 0.5$: a) horizontal component U and b) vertical component V.

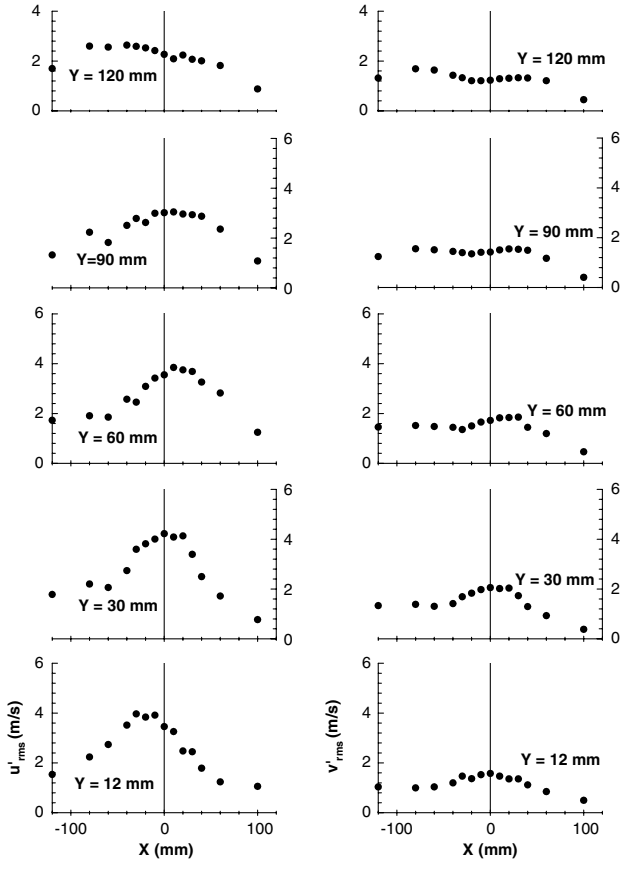

a) b)

Fig. 8 Horizontal profiles of the turbulent velocity characteristics for $V_R = 0.5$: a) horizontal normal stress $\sqrt{\overline{u'^2}}$ and b) vertical normal stress $\sqrt{\overline{v'^2}}$.

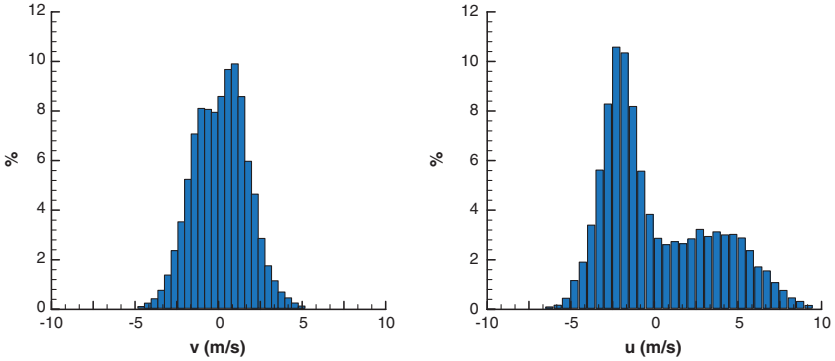

Fig. 9 Typical histograms of the vertical v (LDA1) and horizontal u (LDA2) velocity components at the collision zone ($X = 1$ mm and $Y = 12$ mm) for $V_R = 0.5$.

The velocity ratio was further decreased to $V_R = 0.5$, which corresponds to a puffing frequency of about 5.2 ± 1 Hz, according to [6]. Figure 7 shows horizontal profiles of the mean horizontal U and vertical V velocity components, which confirm the preceding description of the flow and quantify the mean flow characteristics of the collision zone. The mean vertical velocity component (Fig. 7a) is negative for $Y = 12$ and 30 mm and $X > 0$, but is always positive elsewhere. This confirms the existence of the secondary vortex, but it also reveals that when it disappears, it is simply removed upward by the curved flow resulting from the collision between the wall jet and the boundary layer. The profiles of the horizontal velocity show that no significant deflection occurs in the impinging zone ($X = 0$) for $Y < 120$ mm, but for $Y = 90$ to 120 mm, a substantial increase in the vertical velocity component is observed.

From the measured horizontal profiles of the mean velocity component, it can also be observed that the center of the deflected flow cannot be estimated from the zero values of the horizontal velocity component or the maximum values of the vertical velocity component, because they do not coincide. The horizontal velocity component is close to zero at $Y = 90$ mm and $X = 0$, and the maximum vertical velocity component occurs at $X = -40$ mm, but for $Y = 120$ mm, the zero value of U occurs only at $X = -120$ mm and the maximum value of V is only slightly displaced (relative to the case $Y = 90$ mm) in the crossflow direction. This figure also confirms that the center of the secondary-vortex flow is located upstream (in the jet flow sense) of the separation point, probably somewhere before the so-called maximum penetration point (see Fig. 1). This result indicates that this secondary-vortex flow may also be present for the other situations, depending not only on the velocity ratio V_R, but also on the relative size of the clockwise vorticity zone of the wall jet and the counterclockwise vorticity of the boundary layer.

Figure 8 shows horizontal profiles of $\sqrt{\overline{u'^2}}$ and $\sqrt{\overline{v'^2}}$ and quantifies the turbulence characteristics of the collision zone and deflected wall-jet flow. The peaks of $\sqrt{\overline{u'^2}}$ are larger than the corresponding peaks of $\sqrt{\overline{v'^2}}$ in the collision zone, giving rise to high levels of anisotropy with $\sqrt{\overline{u'^2}}/\sqrt{\overline{v'^2}} \approx 2.5$. The maximum values of the horizontal velocity fluctuations are observed in the collision zone in which the mean horizontal velocity component is zero, giving rise to extremely high local turbulence intensity values of $\sqrt{\overline{u'^2}}/U_{\text{mean}}$ greater than 100%. For vertical velocity fluctuations, the maximum values only coincide with the zero values of the mean vertical velocity component close the ground plane ($Y = 12$ mm), and the local turbulence

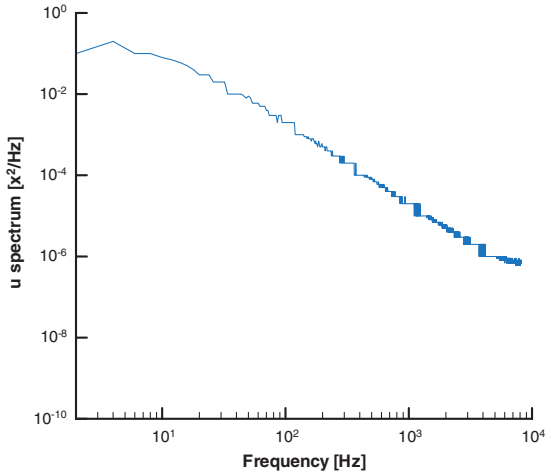

Fig. 10 Power spectra of u corresponding to the measurements shown in Fig. 9 ($X = 1$ mm, $Y = 12$ mm, and $V_R = 0.5$).

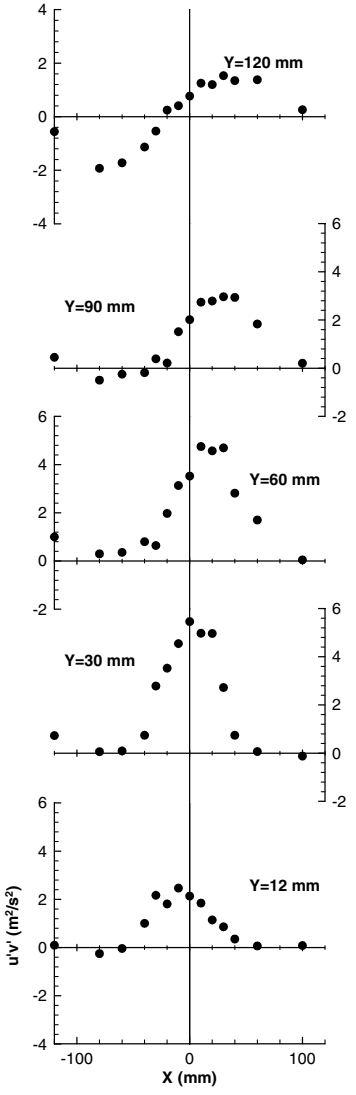

Fig. 11 Horizontal profiles of the turbulent velocity characteristics for $V_R = 0.5$; Reynolds shear stress $\overline{u'v'}$.

intensity is much smaller, although high values such as 40% can be observed, for example, at $Y = 90$ mm and $X = 0$. These results are misleading to some extent, because although the LDV measurements were obtained with a sufficiently high acquisition data rate to detect the possible low-frequency characteristics of these type of instabilities (5.2 ± 1 Hz according to [6]), the total time to obtain the 10,000 measurements needed to keep the statistical errors sufficient low (1.5 and 3%, respectively, for the mean and variance values for a 95% confidence interval [18]) allow the averaging of about 20 cycles. As a consequence, instabilities might be being treated as turbulence, which means that large-scale coherent and turbulent instabilities might be mixed up.

The particular ordered sequence that was identified from the visualization studies for the small recirculation zone that appears near the separation point can also be interpreted as an oscillation of the separation zone or of the virtual deflected-flow origin, which seems to be confirmed by the bimodal histogram of the horizontal velocity measurements obtained in this zone (Fig. 9). In spite of the apparent organized sequence of the turbulent structure of the collision zone, the power spectra of the horizontal velocity component does not exhibit any evident particular peak for the same location (Fig. 10).

The profiles of the shear stress (Fig. 11) are generally consistent with the direction of the mean flow. The shear stress is positive along the vertical direction of the center of the collision zone ($X = 0$), suggesting that faster-moving elements of the wall jet ($u' > 0$) tend to move upward with the deflected upper side of the boundary layer ($v' > 0$). Similarly, the shear stress along the wall-jet side of the deflected flow ($X < -40$ mm) is negative, because the forward movement of fluid particles corresponds to negative vertical velocity fluctuations ($v' < 0$). However, far from the ground, the locations of the zero values of the shear stress occur in the neighborhood of $X = 0$ (for example, $X = -40$ mm for $Y = 90$ mm), but do not coincide with the central zone of the deflected flow, which is associated with the maximum of the vertical velocity component, where $\partial V/\partial X = 0$. Far from the wall ($Y > 25$ mm) with the approach of the separation point ($X = 0$), $\partial U/\partial Y$ increases on the wall-jet side ($X < 0$) and decreases on the boundary-layer side ($X > 0$). Near the wall, $\partial V/\partial y$ and $\partial U/\partial X$ are the most important shear strains, and the magnitude of the peak of the shear stress decreases. This is because the flow in this region is subjected to strongly stabilizing curvature that reduces the shear stress more than the turbulent kinetic energy.

Figure 12 shows measured vertical profiles of the mean velocity components U and V and reveals the presence of the small vortex in

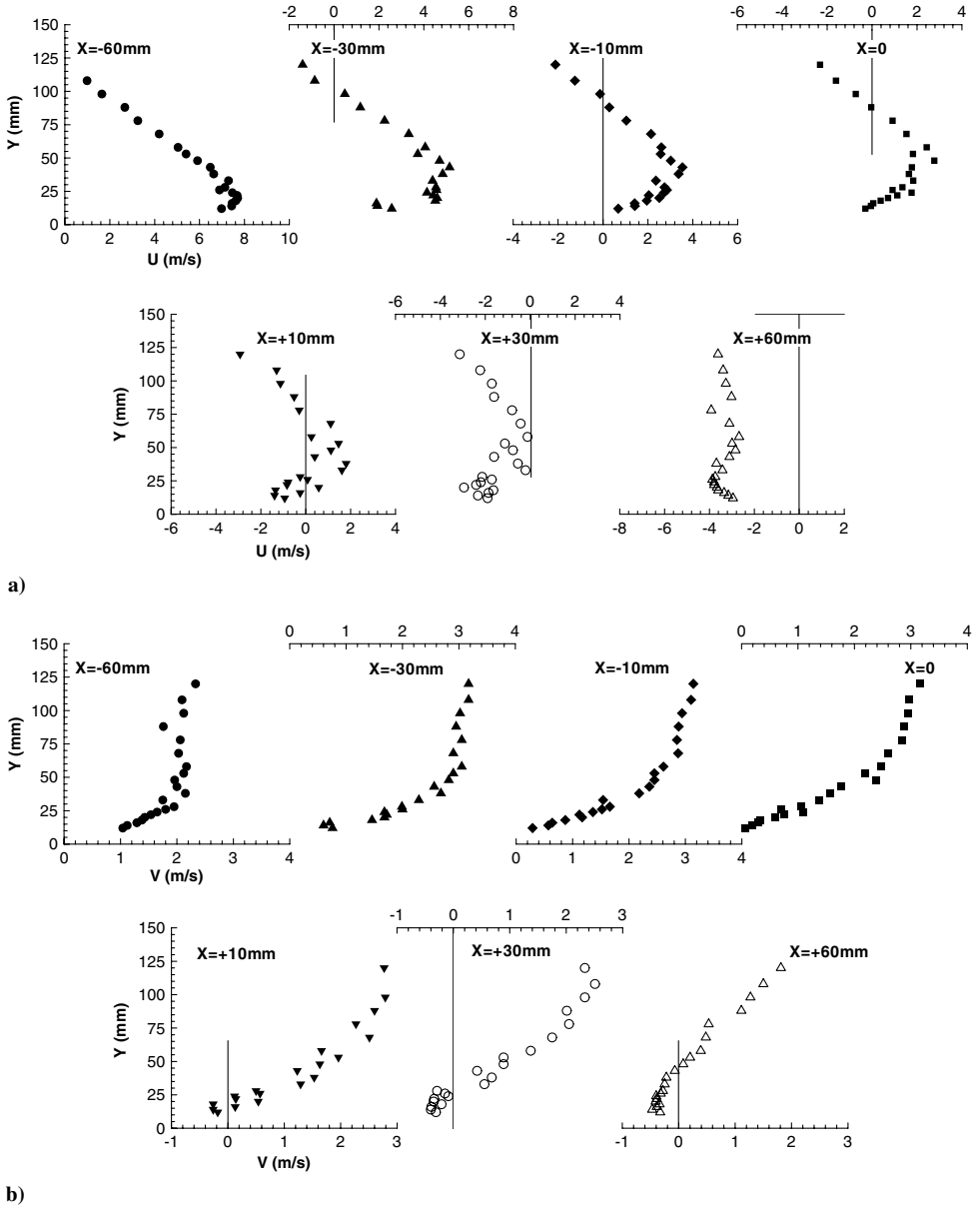

Fig. 12 Vertical profiles of the mean velocity characteristics for $V_R = 0.5$: a) horizontal component U and b) vertical component V.

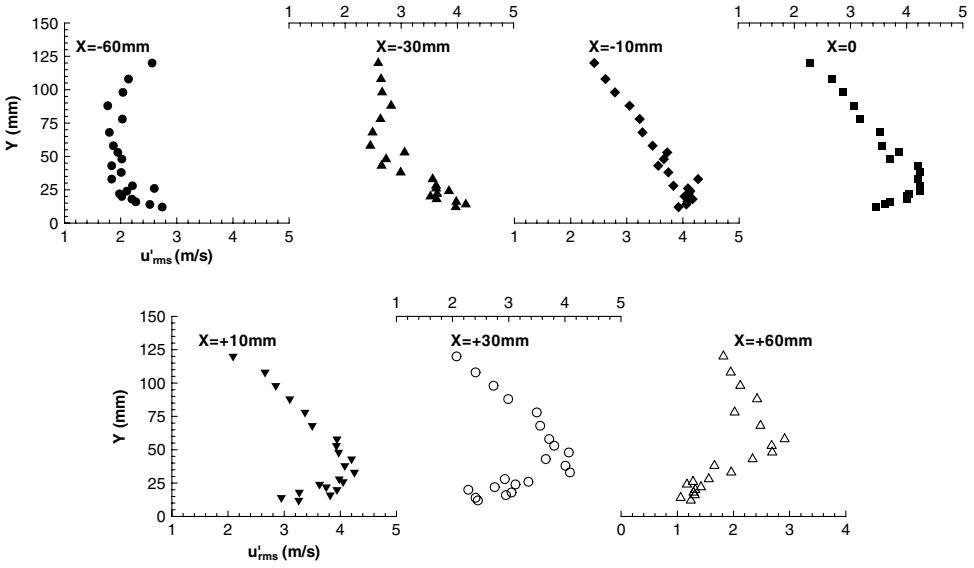

a)

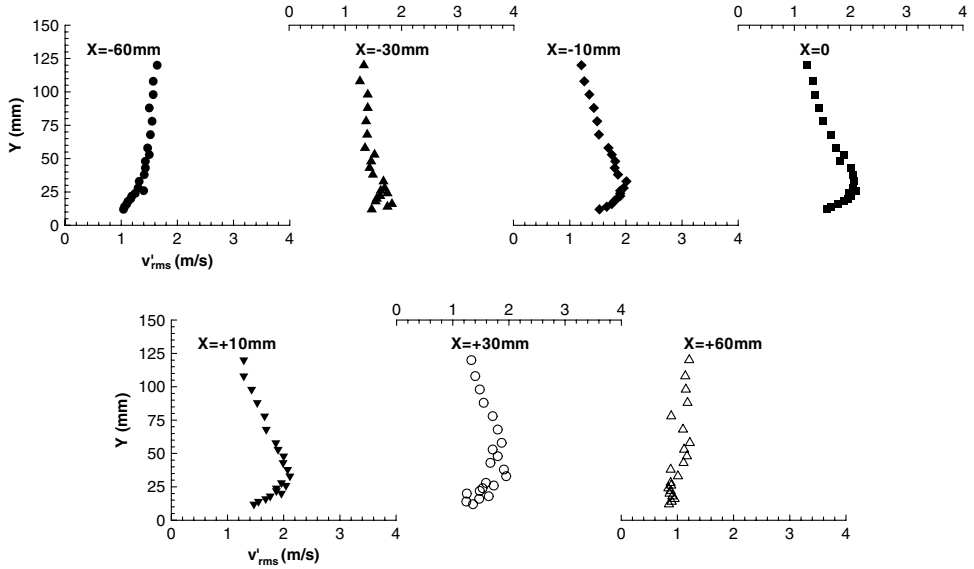

b)

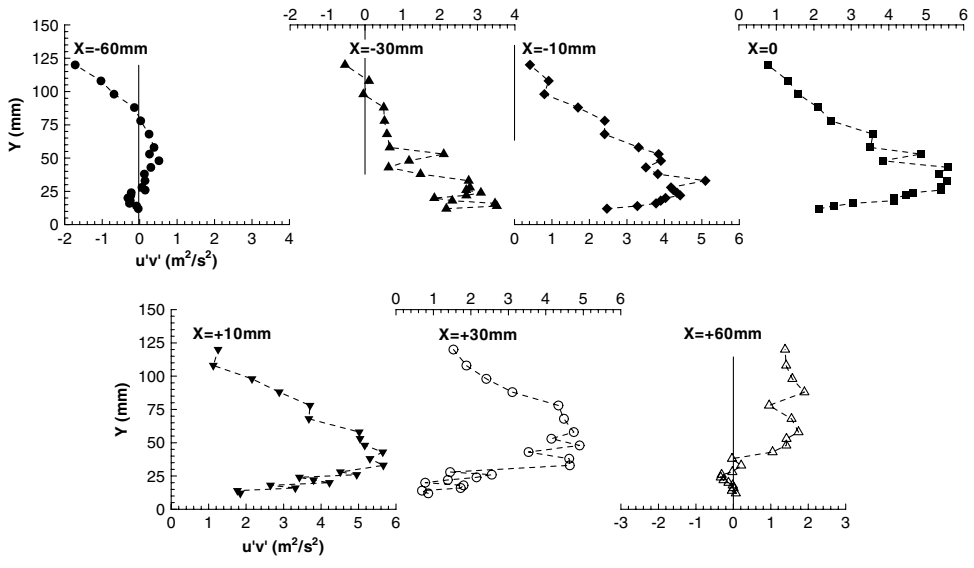

c)

Fig. 13 Vertical profiles of the turbulent velocity characteristics for $V_R = 0.5$: a) horizontal normal stress $\sqrt{\overline{u'^2}}$, b) vertical normal stress $\sqrt{\overline{v'^2}}$, and c) shear stress $\overline{u'v'}$.

the boundary-layer side of the separation point ($X > 0$) in the profiles at $X = +10$, $+30$, and $+60$ mm. The vertical V velocity component changes its sign with the distance to the wall, with negative values of V (i.e., downward) close to the wall, revealing the existence of the counterclockwise vorticity in the collision zone already discussed in the previous paragraphs (see also Fig. 4).

The vertical profiles of the turbulent velocity characteristics (Fig. 13) also show the high turbulent intensities measured in the collision zone near the wall at $X = 0$. It should be pointed out that the histograms of the measured horizontal velocity component are bimodal near the wall, with the dominant peak located on the negative or positive side, depending on the location of the measuring point. The bimodal histograms are also associated with the larger dispersion of the measurements near the wall ($Y = 0$) and the separation point ($X = 0$), because the number of measurements was maintained constantly equal to 10,000.

IV. Conclusions

Laser-Doppler measurements of the velocity characteristics of two-dimensional ground-vortex flows resulting from the collision of a wall jet with a boundary layer were presented and discussed with visualization results for boundary-layer-to-wall-jet velocity ratios of 0.5 and 0.58.

The results revealed the existence of a small-vortex flow located upstream (in the wall-jet flow sense) of the separation point, not yet reported before for this type of flow.

The secondary vortex has a similar very-low-broadband pulsating behavior by expanding and contracting observed in some impinging-jet configurations with ground-vortex flows. First, the vortex is very small but growing. The lower part of the boundary layer with anticlockwise vorticity seems to merge into the growing vortex. As the small vortex continues to grow, it becomes higher than the boundary layer and breaks up suddenly while is convected upward in the direction of the curved flow. Then a new small vortex appears and starts to grow, and the cyclic process repeats itself.

The secondary-vortex growth cannot be attributed to the shear-layer vortices, which convect with the wall jet, because it cannot merge into the deflected flow resulting from the collision of the wall jet with the boundary layer, because the vertical velocity component is always positive above the vortex.

The unsteadiness of the ground vortex reported before for the case of impinging jets in unconfined crossflows may also be associated with an additional small-vortex upstream separation point, but due to its extremely small size it could not be observed so far, as in the case of very small crossflow-to-jet velocity ratios.

The particular ordered sequence that was identified from the visualization studies for the small recirculation zone that appears near the separation point can also be interpreted as an oscillation of the separation zone or of the virtual deflected-flow origin and can be confirmed by the bimodal histogram of the horizontal velocity measurements obtained in this zone. In spite of the apparent organized sequence of the turbulent structure of the collision zone, the power spectra of the horizontal velocity component does not exhibit any evident particular peak for the same location.

Acknowledgments

The financial support of the Fundação para a Ciência e Tecnologia (FCT) of the Portuguese Ministry of Science under contract no. PTDC/EME/-MFE/64493/2006 is gratefully acknowledged. The present work has been performed in the scope of the activities of the Aeronautics and Astronautics Research Center—AeroG of the University of Beira Interior.

References

[1] Castro, I. P., and Bradshaw, P., "The Turbulence Structure of a Highly Curved Mixing Layer," *Journal of Fluid Mechanics*, Vol. 73, Part 2, 1976, pp. 265–304. doi:10.1017/S0022112076001377

[2] Barata, J. M. M., Durão, D. F. G., and Heitor, M. V., "Experimental and Numerical Study on the Aerodynamics of Jets in Ground Effect," *Tenth Symposium on Turbulence*, Rolla, MO, Sept. 1986.

[3] Barata, J. M. M., Durão, D. F. G., and Heitor, M. V., "The Turbulent Characteristics of a Single Impinging Jet Through a Crossflow," *Sixth Symposium on Turbulent Shear Flows*, Toulouse, Sept. 1987.

[4] Barata, J. M. M., Durão, D. F. G., and Heitor, M. V., "Turbulent Energy Budgets in Impinging Zones," *Eighth Symposium on Turbulent Shear Flows*, Munich, Sept. 1991.

[5] Van Dalsem, W. R., Panaras, A. G., and Steger, J. L., "Numerical Investigation of a Jet in a Ground Effect with a Crossflow," International Powered Lift Conference, Santa Clara, CA, Society of Automotive Engineers Paper 872344, Dec. 1987.

[6] Cimbala, J. M., Billet, M. L., Gaublomme, D. P., and Oefelein, J. C., "Experiments on the Unsteadiness Associated with a Ground Vortex," *Journal of Aircraft*, Vol. 28, No. 4, Apr. 1991, pp. 261–267. doi:10.2514/3.46021

[7] Knowles, K., and Bray, D., "The Ground Vortex Formed by Impinging Jets in Crossflow," AIAA 29th Aerospace Sciences Meeting, Reno, NV, AIAA Paper 91-0768, Jan. 1991.

[8] Saripalli, K. R., "Laser Doppler Velocimeter Measurements in 3D Impinging Twin-Jet Fountain Flows," *Turbulent Shear Flows*, Vol. 5, Springer–Verlag, Berlin, 1987, pp. 147–168.

[9] Saripalli, K. R., "Visualization of Multijet Impingement Flow," *AIAA Journal*, Vol. 21, No. 4, 1983, pp. 483–484. doi:10.2514/3.8102

[10] Saddington, A. J., Knowles, K., and Cabrita, P. M., "Flow Visualization and Measurements in a Short Takeoff, Vertical Landing Fountain Flow," 45th AIAA Aerospace Sciences Meeting and Exhibit, Reno, NV, AIAA Paper 2007-1402, Jan. 2007.

[11] Barata, J. M. M., Durão, D. F. G., and Heitor, M. V., "Impingement of Single and Twin Turbulent Jets Through a Crossflow," *AIAA Journal*, Vol. 29, No. 4, Apr. 1991, pp. 595–602. doi:10.2514/3.10626

[12] Barata, J. M. M., "Ground Vortex Formation with Twin Impinging Jets," International Powered Lift Conference, Jupiter, FL, Society of Automotive Engineers Paper 962257, Nov. 1996.

[13] Barata, J. M. M., "Fountain Flows Produced by Multiple Jets in a Crossflow," *AIAA Journal*, Vol. 34, No. 12, Dec. 1996, pp. 2523–2530. doi:10.2514/3.13434

[14] Barata, J. M. M., and Durão, D. F. G., "Laser-Doppler Measurements of Impinging Jets Through a Crossflow," *Experiments in Fluids*, Vol. 36, No. 5, 2004, pp. 117–129.

[15] Gilbert, B. L., "Detailed Turbulence Measurements in a Two-Dimensional Upwash," 16th AIAA Fluid and Plasma Dynamics Conference, Danvers, MA, AIAA Paper 83-1678, July 1983.

[16] Barata, J. M. M., and Durão, D. F. G., "Laser-Doppler Measurements of a Highly Curved Flow," *AIAA Journal*, Vol. 43, No. 12, Dec. 2005, pp. 2652–2655. doi:10.2514/1.14846

[17] Metha, R. D., and Bradshaw, P., "Design Rules for Small Low-Speed Wind Tunnels," *The Aeronautical Journal*, Vol. 73, Nov. 1979, pp. 443–449.

[18] Yanta, Z., and Smith, R. A., "Measurements of Turbulent-Transport Properties with Laser-Doppler Velocimeter," 11th Aerospace Sciences Meeting, Washington, D.C., AIAA Paper 73-0169, 1973.